Interhemispherical asymmetry of substorm onset locations and the interplanetary magnetic field

N. Østgaard,[1] K. M. Laundal,[2] L. Juusola,[1] A. Åsnes,[3] S. E. Håland,[1,4] and J. M. Weygand[5]

Received 13 January 2011; revised 16 February 2011; accepted 21 February 2011; published 23 April 2011.

[1] The auroral substorm display in the conjugate hemispheres offers a unique tool to understand how the Earth's plasma and magnetic environment respond to changes in the solar wind and the interplanetary magnetic field (IMF). Earlier studies have demonstrated that substorm onset locations in the two hemispheres are systematically displaced due to the orientation of the IMF, but it is still a controversy which IMF parameter is most important. We have analysed more than 6600 substorms identified from global auroral images by Polar UVI from years 1996–2000 plus 2007 and IMAGE FUV from years 2000–2005. We find very strong statistical support for earlier conjugate auroral imaging observations, according to which the IMF clock angle, θ_c, organizes the average substorm onset locations in both hemispheres. The IMF θ_c control is a manifestation of dayside/lobe reconnection geometry and magnetic tension on open field lines before tail reconnection resulting in closed field lines with asymmetric footpoints for all θ_c angles. By organizing the average substorm locations by the IMF B_y component only we also find statistical significance. The relation is not linear, as reported earlier, but reveals saturation effects that can be explained by the non-uniform penetration of IMF B_y into the closed magnetosphere. **Citation:** Østgaard, N., K. M. Laundal, L. Juusola, A. Åsnes, S. E. Håland, and J. M. Weygand (2011), Interhemispherical asymmetry of substorm onset locations and the interplanetary magnetic field, *Geophys. Res. Lett.*, *38*, L08104, doi:10.1029/2011GL046767.

1. Introduction

[2] When and why the auroras are asymmetric in the two hemispheres are key questions that need to be answered to obtain a more complete knowledge on how the Earth's plasma and magnetic environment interacts and responds to changes in the solar wind and the interplanetary magnetic field (IMF).

[3] As a contribution to this effort *Østgaard et al.* [2004, 2005] have previously reported, based on simultaneous conjugate auroral images, that the locations of the auroral substorm onset in the conjugate hemispheres are usually not symmetric. Although these studies were based on a limited number of events (15) they indicated clearly that the degree of asymmetry is well correlated with the orientation of the IMF. Comparing the degree of asymmetry with the IMF clock angle (θ_c) and the IMF B_y component, they found that IMF θ_c gives a slightly higher correlation coefficient than comparing with the IMF B_y only. θ_c is defined as the angle between the IMF and Z-axis in the YZ plane of the Geocentric Solar Magnetospheric (GSM) reference system. The observed asymmetry was also found to be larger than predicted by the empirical magnetic field models [*Østgaard et al.*, 2005].

[4] We suggested that the IMF θ_c control can be understood as the magnetic stress imposed by the IMF on the Earth's magnetic field from the moment the field lines are opened on the dayside, draped down the tail and until they eventually close through reconnection in the mid-tail before substorm onset. The result of this tension force on open field lines is that only the ones with asymmetric footpoints will reconnect in the mid-tail forming closed field lines with interhemispherically asymmetric footpoints [*Østgaard et al.*, 2005]. To explain how IMF B_y affects the substorm onset location one would rather consider the asymmetric cross-tail pressure resulting from a non-zero IMF B_y that non-uniformly penetrates into the closed magnetosphere [*Cowley*, 1981; *Khurana et al.*, 1996].

[5] The identification of a large number of substorms in both hemispheres from IMAGE FUV data [*Frey et al.*, 2004] provided an opportunity to confirm statistically the results of previous event studies. Based on more than 3700 substorms identified from 2000 to 2004, *Østgaard et al.* [2007] showed that the IMF clock angle control of the asymmetry of substorm onset location is indeed statistically significant. *Wang et al.* [2007] analysed an extended version of this list [*Frey and Mende*, 2006] of substorms from IMAGE including the year 2005, giving a total of 4192 substorms. Although they mainly focused on the IMF B_y and the solar zenith effect, they also reported that no IMF θ_c control of substorm onset location could be found in the data. Unfortunately, no results were shown and they did not explain how they performed the unsuccessful search for a IMF θ_c control.

[6] In a recent paper *Liou and Newell* [2010] analysed a new set of substorms identified from Polar UVI data [*Liou*, 2010]. This substorm list is complementary to the IMAGE list and covers the years from 1996 to 2000 and 2007. Their main result is that substorm onset locations have a dependence on the pairing of IMF B_y/tilt angle, which is a confirmation of what was suggested by *Østgaard et al.* [2005, Figure 1], where $\theta_c = 90°$ (positive B_y) and positive tilt angle (northern summer) gives the largest positive ΔMLT which implies the earliest substorms in northern hemisphere. *Liou*

[1]Department of Physics and Technology, University of Bergen, Bergen, Norway.
[2]Teknova, Kristiansand, Norway.
[3]Bergen Oilfield Services, Bergen, Norway.
[4]Max-Planck Institute, Katlenburg-Lindau, Germany.
[5]Institute of Geophysics and Planetary Physics, University of California, Los Angeles, California, USA.

0094-8276/11/2011GL046767

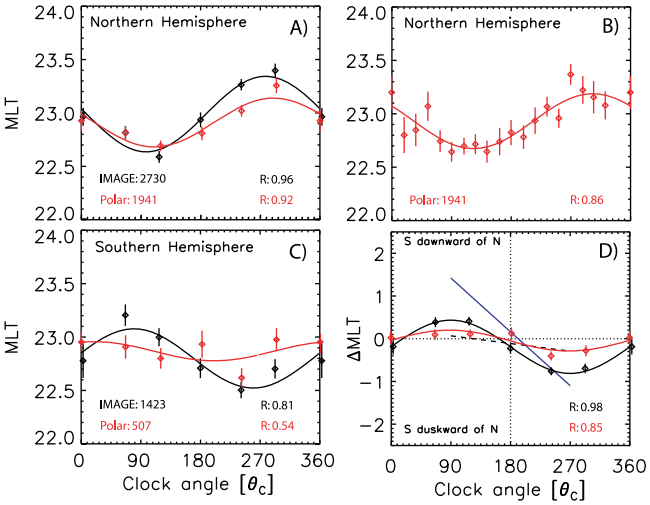

Figure 1. (a) Substorm MLT locations for 60° bins of IMF θ_c in the northern hemisphere. Substorms identified from IMAGE (Polar) data are shown in black (red). (b) Average substorm MLT locations for 18° bins of IMF θ_c for substorms identified from Polar data in the northern hemisphere. (c) Same as Figure 1a for southern hemisphere. Total number of substorms are shown in lower left corner of Figures 1a–1c. (d) ΔMLT between the southern and northernaverage substorm locations. The blue line shows the result we obtained from simultaneous conjugate auroral images and the dashed line is what empirical magnetic field models predict [*Tsyganenko*, 2002]. The error bars in all panels are the standard deviations of the mean values. R_S is the Spearman correlation coefficient between the data and a sine function.

and Newell [2010] found a similar dependence on the pairing of IMF B_y/solar zenith angle, consistent with the results from *Wang et al.* [2007]. They also found a weak IMF θ_c control of substorm onset location, but still argue that this is not a strong controlling parameter for substorm onset location.

[7] Motivated by the findings (or the lack thereof) in these two studies [*Wang et al.*, 2007; *Liou and Newell*, 2010] and the release of a new and complementary substorm list based on Polar UVI data [*Liou*, 2010], we find it important to revisit this problem and try to settle the controversy. We will first compare the results from the two substorm lists applying exactly the same method to both data sets. Then we will use the entire data set of more than 6600 substorms to investigate how the relation between the IMF parameters, θ_c and B_y, and substorm onset location can give us a better understanding of how the IMF interacts with the Earth's magnetic fields and plasma. To make our results as transparent as possible, we have uploaded a file with all the substorm times, MLT locations and the corresponding IMF data as auxiliary material.[1]

2. Data

[8] We have used the extended substorm list from IMAGE FUV data comprising 4192 substorms from years 2000 to 2005 and the new substorm list from Polar UVI data comprising 2539 substorms. The solar wind data are mainly from ACE but using Wind when ACE is not available. The data have been time shifted to X = $17R_E$ using the propagation method described by *Weimer* [2004]. These data can be downloaded from measure.igpp.ucla.edu. The data have been further time shifted using planar propagation from X = $17R_E$ to X = $-10R_E$ (average of ±5 min and 40 minutes prior to onset time) and X = $-20R_E$ (average of +−5 min) to investigate different possible impact times from the solar wind to the magnetosphere.

3. Results

[9] For each of the data sets we have grouped the substorm locations in 60° bins of IMF θ_c and calculated the average substorm onset location in each bin, as well as the standard deviation of each bin-average. Throughout this paper average refers to the arithmetic mean. The results are shown in Figure 1 where the data from IMAGE and Polar are shown in black and red, respectively. A sine function with three free parameters, $Y = A_0 \sin(\theta_c + A_1) + A_2$, is fitted to the data, where Y = MLT in Figures 1a–1c and Y = ΔMLT in Figure 1d. From the IMAGE data one can clearly see that the average substorm location in the northern (Figure 1a) and southern (Figure 1c) hemisphere are in anti-phase and that the relative asymmetry (Figure 1d) follows a sine function. The Spearman correlation coefficients (R_S) for these fits are 0.96 (north), 0.81 (south) and 0.98 (relative). The error bars are the standard deviation of each bin-average, which implies that for a new and independent sample of substorms, we would expect, on average, that 2/3 of the data points should be within the error bars.

[10] For the northern hemisphere (Figure 1a), the number of substorms in each bin is large for both data sets, varying from 120 to 479 for Polar and from 174 to 665 for IMAGE. The sine functional fit is good (R = 0.92) also for Polar, and only one of the values ($\theta_c \sim 240°$) does not have overlapping error bars with the IMAGE data. For the southern hemisphere (Figure 1c), the number of substorms in each bin is significantly smaller for Polar (40–120) than for IMAGE (68–340). Consequently, the sine functional fit is poor (R = 0.54) for Polar, although only two data points ($\theta_c \sim 60°$ and ~290°) do not have overlapping error bars with the IMAGE data, indicating that the new data are within the statistical expectations. For the relative displacement (Figure 1d), four pairs of points do not overlap. The sine functional fit, on the other hand, is good (R = 0.85). The Polar data with the same resolution (18° bins) as was used by *Liou and Newell* [2010] are shown in Figure 1b. With the higher resolution the number of samples in each bin is smaller, but the sine function still fits the data set very well (R = 0.86).

[11] In Figures 2a–2c we show the IMF θ_c control of substorm onset location for the combined data set which covers 6601 substorms from the years 1996–2005 plus 2007. Due to the larger number of substorms we have used 30° bins of IMF θ_c. The number of substorms in each bin ranges from 89 to 620 and 33 to 240 in the northern and southern hemisphere, respectively. The different time-shifts and averaging (black, red and blue diamonds) give almost similar results. The sine functional fits show how the average substorm locations in the two hemisphere are in anti-phase.

[1] Auxiliary materials are available at ftp://ftp.agu.org/apend/gl/2011gl046767.

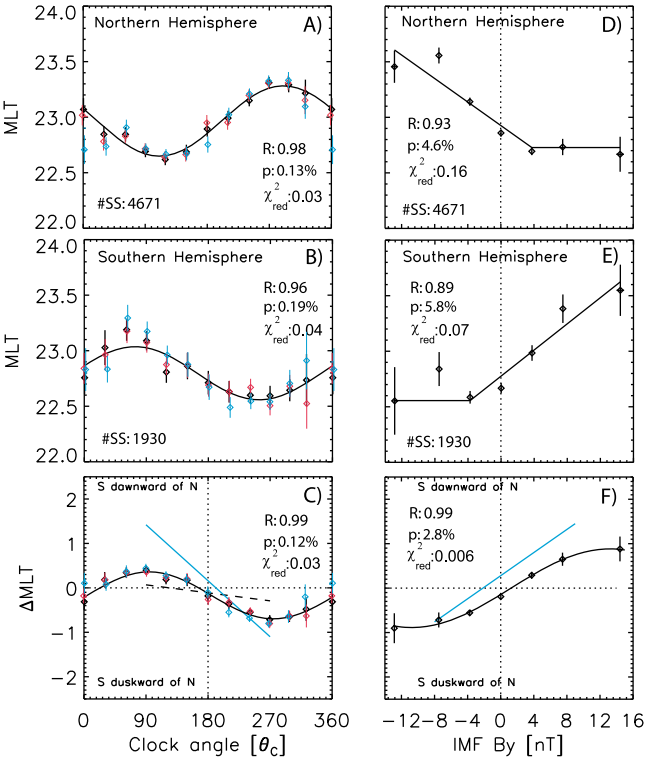

Figure 2. (a–c) Same as Figure 1 but for the combined IMAGE and Polar data sets. 30° bins of IMF θ_c have been used. Black, red and blue diamonds are for time shifts to $-10R_E$/±5 min, $-20R_E$/±5 min and $-10R_E$/40 min. (d–f) Same as Figures 2a–2c, but the substorm onset MLTs have been organized in 4 nT bins of IMF B_y (only time shifts to $-10R_E$/±5 min). The blue straight lines in Figures 2c and 2f are the linear fits from *Østgaard et al.* [2005]. The error bars in all panels are standard deviation of the mean values.

The best correlations are found for $-10R_E$ and ±5 min, with R_S of 0.98 (north), 0.96 (south) and 0.99 (relative).

[12] Finally we show (Figures 2d–2f) how the average substorm locations are related to IMF B_y using the combined data set from Image and Polar. Despite the larger number of substorms the sampling for large $|B_y|$ values are poor. We have therefore used 4 nT bin resolution and integral < -10 nT and >10 nT, giving number of substorms in each bin that ranges from 61 to 1427 in the northern hemisphere and 24 to 753 in the southern hemisphere. Neither the northern or the southern hemisphere reveals a linear relation, but rather a linear relation for negative (positive) B_y in the northern (southern) hemisphere and a constant value (saturation effect) for positive (negative) B_y in the North (South), giving R_S = 0.93 (north) and R_S = 0.82 (south). The asymmetry between hemispheres is very well fitted with a sine function (R_S = 0.99).

4. Discussion and Summary

[13] Our results (Figure 1) show clearly that the average substorm onset locations in the two hemispheres based on the IMAGE FUV list of substorms follow a sine function of IMF θ_c and that the two hemispheres are in anti-phase. When analysing the new and complementary substorm list based on Polar UVI data we find that the distribution of average substorm onset location follows a similar sine function in the northern hemisphere, where the number of data points are comparable, giving a high correlation coefficient of 0.92. Due to the much smaller data set from Polar in the southern hemisphere we do not see a clear sine function in anti-phase to the northern hemisphere. However, as less than 1/3 of the data points are outside the standard deviation, the distributions from Polar are still statistically in agreement with the IMAGE distributions in this hemispheres as well. We have also shown that the sine distribution for the substorms in northern hemisphere from Polar is statistically significant when using similar bins as *Liou and Newell* [2010] (R = 0.86).

[14] Our average IMF θ_c estimates are not the same as reported by *Liou and Newell* [2010, Figure 1D] and may indicate that the time-shifted OMNI data and the UCLA data are not the same.

[15] As a check, we have compared the θ_c values for 2007 (~540 substorms) and found that 39% (21%) of the OMNI θ_c values differ more than 30° (60°) from the UCLA values. There might be other differences in analysis performance as well. However, we find it extremely unlikely that errors in data processing on our side should coincidentally show up as a statistically significant correlation. We would rather think that errors in the procedure would scramble the data and remove statistical significance.

[16] When analysing the combined data set the IMF θ_c control becomes even clearer, with $R_S > 0.96$, probability, $p < 0.2\%$, and $\chi^2_{red} < 0.05$ leaving little doubt that the average onset locations and interhemispheric asymmetry are organized as a sine function of IMF θ_c. Although different time shifts and averaging (red and blue diamonds in Figures 2a–2c) give almost similar results, the correlation is significantly poorer for 40 min averaging with R_S down to 0.75, p as high as 1.8% and χ^2_{red} of 0.3. Time shifts to $-10R_E$ give slightly better correlation than for $-20R_E$. The IMF θ_c control (black diamonds in Figures 2a–2c) can be summarized in the following three equations (subscripts refer to north and south).

$$MLT_n = 0.32 \times \sin(\theta_c - 201) + 22.9, \quad (1)$$

$$MLT_s = 0.24 \times \sin(\theta_c + 16.3) + 22.8 \quad (2)$$

$$\Delta MLT\,(MLT_s - MLT_n) = 0.53 \times \sin(\theta_c - 4.8) - 0.17 \quad (3)$$

If only values with total IMF larger than 5 nT are included the amplitudes increase to 0.41 (north), 0.35 (south) and 0.73 (relative), while the phase shifts and constants are unchanged. Due to fewer data points the errors are larger.

[17] These results give a very strong support to the results reported by *Østgaard et al.* [2004, 2005]. These studies were limited to only southward IMF and we explained the IMF θ_c control by the magnetic stress imposed by the IMF on the Earth's magnetic field from the moment the field lines are opened on the dayside, draped down the tail and until they eventually close through reconnection in the mid-tail before substorm onset. Now we observe that the IMF θ_c control is also apparent for substorms during northward IMF, under which conditions no magnetic flux is opened by lobe reconnection. However, open field lines can still be closed by tail

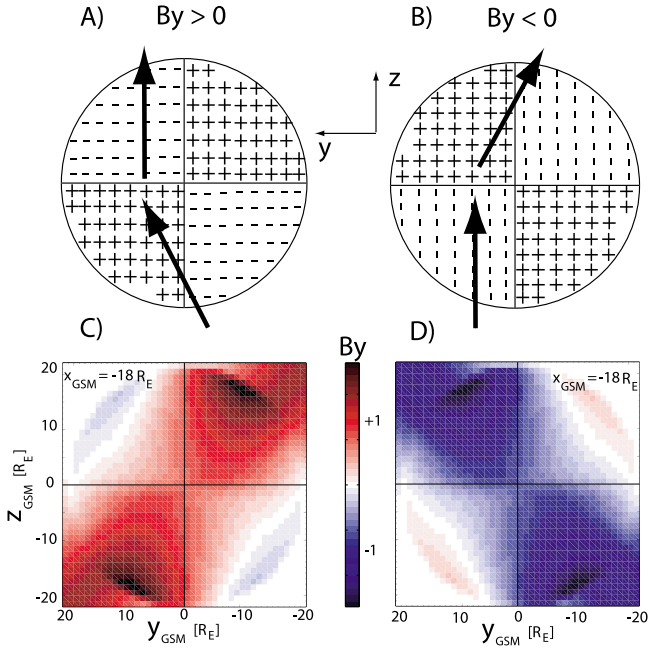

Figure 3. (a) For IMF $B_y > 0$, + (−) indicates where magnetic flux is added (not added) for IMF $B_y > 0$. Arrows indicate how closed magnetic fields can be affected in the dusk sector. (b) Same as Figure 3a but for IMF $B_y < 0$. (c and d) Results from Tsyganenko 96 model showing how the IMF $B_y = \pm 3$ nT non-uniformly penetrates the magnetotail.

reconnection [*Cowley and Lockwood*, 1992; *Grocott et al.*, 2005]. Thus, due to the tension force imposed by IMF before tail reconnection the resulting closed field lines will, also in this case, have asymmetric footpoints. The sine behavior with maxima at $\theta_c = 90°/270°$ (Figure 2c) is exactly what one would expect from considering dayside and lobe reconnection geometry and tension force on open field lines.

[18] Our results are all based on average values and cannot be used to predict the location of one single substorm. However, the relative displacement (equation (3)) is probably a more robust result that can be used when the location in one hemisphere is known [e.g., *Motoba et al.*, 2010]. Although unbinned data have a large spread they can still be fitted by sine functions (not shown).

[19] The comparison between average substorm location and IMF B_y also gives results that are statistically significant and provides additional information about the interaction between the IMF and the closed magnetosphere. The relation is not linear, as previously reported [*Østgaard et al.*, 2005; *Wang et al.*, 2007; *Liou and Newell*, 2010], but reveals a saturation effect for positive (negative) B_y values in the North (South).

[20] This effect can be explained by considering how magnetic flux is added non-uniformly to the magnetotail for negative and positive By values [*Khurana et al.*, 1996], and assuming that this non-uniform penetration of IMF By extends into the closed magnetosphere. We have illustrated this in Figure 3a by sketching the cross section of the magnetotail and how magnetic flux is added (+) in the northern dawn and the southern dusk for IMF $B_y > 0$. This means that a positive B_y will penetrate only in the southern dusk and a negative B_y will only penetrate into the northern dusk. Considering also that substorms on average are located in the pre-midnight region, the closed magnetic field lines (arrows) will be affected by $B_y > 0$ in the southern hemisphere and not in the northern, where we observe the saturation effect for $B_y > 0$. For $B_y < 0$ (Figure 3b) it is opposite. The flux is not added to the southern dusk, consistent with the saturation we observe in the southern hemisphere for $B_y < 0$. This idea is supported by results from the semi-empirical Tsyganenko 96 model (Figures 3c and 3d). The interhemispherical asymmetry is related to B_y as

$$\Delta MLT\ (MLT_s - MLT_n) = 0.88\ \times\ \sin\left(\frac{B_y}{12nT} - 9.3\right) \qquad (4)$$

To summarize, based on more than 6600 substorm onset locations identified by Polar UVI and IMAGE FUV covering the years from 1996 to 2005 plus 2007 we have found the following:

[21] 1. The IMF θ_c controls the average substorm locations in both hemispheres and explains the asymmetry of onset locations between the hemispheres. This is a manifestation of dayside and lobe reconnection geometry and magnetic tension on open field lines before tail reconnection resulting in closed field lines with asymmetric footpoints and is valid for all θ_c angles.

[22] 2. The relation between IMF B_y and the average substorm locations is also statistically significant. It is not linear, but reveals a saturation effect due to the non-uniform penetration of IMF B_y into the closed magnetosphere. The interhemispherical asymmetry is very well correlated with B_y.

[23] **Acknowledgments.** We thank H. U. Frey and K. Liou for identifying substorm onset locations from IMAGE FUV images and Polar UVI images, respectively. We thank R. Lepping for the WIND magnetic field data, A. Lazarus for the WIND solar wind data, C. Smith for the ACE magnetic field data and D. McComas for the ACE solar wind data. This study was supported by the Norwegian Research Council, through the IPY-ICESTAR project 176045/S30.

[24] The Editor thanks Alan Rodger and an anonymous reviewer for their assistance in evaluating this paper.

References

Cowley, S. W. H. (1981), Magnetospheric asymmetries associated with the Y-component of the IMF, *Planet. Space Sci.*, *29*, 79–96.

Cowley, S. W. H., and M. Lockwood (1992), Excitation and decay of solar wind-driven flows in the magnetosphere-ioneosphere system, *Ann. Geophys.*, *10*, 103–115.

Frey, H. U., and S. B. Mende (2006), Substorm onset as observed by IMAGE-FUV, in *Proceedings of the 8th International Conference on Substorms*, edited by M. Syrjäsuo and E. Donovan, pp. 71–76, Univ. of Calgary, Calgary, Alberta, Canada.

Frey, H. U., S. B. Mende, V. Angelopoulos, and E. F. Donovan (2004), Substorm onset observations by IMAGE-FUV, *J. Geophys. Res.*, *109*, A10304, doi:10.1029/2004JA010607.

Grocott, A., T. K. Yeoman, S. E. Milan, and S. W. H. Cowley (2005), Interhemispheric observations of the ionospheric signature of tail reconnection during IMF-northward non-substorm intervals, *Ann. Geophys.*, *23*, 1763–1770.

Khurana, K. K., R. J. Walker, and T. Ogino (1996), Magnetospheric convection in the presence of interplanetary magnetic field B_y: A conceptual model and simulations, *J. Geophys. Res.*, *101*, 4907–4916, doi:10.1029/95JA03673.

Liou, K. (2010), Polar Ultraviolet Imager observation of auroral breakup, *J. Geophys. Res.*, *115*, A12219, doi:10.1029/2010JA015578.

Liou, K., and P. T. Newell (2010), On the azimuthal location of auroral breakup: Hemispheric asymmetry, *Geophys. Res. Lett.*, *37*, L23103, doi:10.1029/2010GL045537.

Motoba, T., K. Hosokawa, N. Sato, A. Kadokura, and G. Bjornsson (2010), Varying interplanetary magnetic field By effects on interhemispheric conjugate auroral features during a weak substorm, *J. Geophys. Res.*, *115*, A09210, doi:10.1029/2010JA015369.

Østgaard, N., S. B. Mende, H. U. Frey, T. J. Immel, L. A. Frank, J. B. Sigwarth, and T. J. Stubbs (2004), Interplanetary magnetic field control of the location of substorm onset and auroral features in the conjugate hemispheres, *J. Geophys. Res.*, *109*, A07204, doi:10.1029/2003JA010370.

Østgaard, N., N. A. Tsyganenko, S. B. Mende, H. U. Frey, T. J. Immel, M. Fillingim, L. A. Frank, and J. B. Sigwarth (2005), Observations and model predictions of substorm auroral asymmetries in the conjugate hemispheres, *Geophys. Res. Lett.*, *32*, L05111, doi:10.1029/2004GL022166.

Østgaard, N., S. B. Mende, H. U. Frey, J. B. Sigwarth, A. Aasnes, and J. M. Weygand (2007), Auroral conjugacy studies based on global imaging, *J. Atmos. Sol. Terr. Phys.*, *69*, 249–255, doi:10.1016/j.jast9.2006.05.026.

Tsyganenko, N. A. (2002), A model of the near magnetosphere with a dawn-dusk asymmetry: 2. Parameterization and fitting to observations, *J. Geophys. Res.*, *107*(A8), 1176, doi:10.1029/2001JA000220.

Wang, H., H. Lühr, S. Y. Ma, and H. U. Frey (2007), Interhemispheric comparison of average substorm onset locations: Evidence for deviation from conjugacy, *Ann. Geophys.*, *25*, 989–999.

Weimer, D. R. (2004), Correction to "Predicting interplanetary magnetic field (IMF) propagation delay times using the minimum variance technique," *J. Geophys. Res.*, *109*, A12104, doi:10.1029/2004JA010691.

A. Åsnes, Bergen Oilfield Services, Nedre Åstveit 12, N-5106 Bergen, Norway.

S. E. Håland, L. Juusola, and N. Østgaard, Department of Physics and Technology, University of Bergen, Allegt. 55, N-5007 Bergen, Norway. (nikolai.ostgaard@ift.uib.no)

K. M. Laundal, Teknova, Gimlemoen 19, N-4630 Kristiansand, Norway.

J. M. Weygand, Institute of Geophysics and Planetary Physics, University of California, 3845 Slichter Hall, 405 Charles E. Young Dr., Los Angeles, CA 90095-1567, USA.